

Low Cation Coordination in Oxide Melts

L. B. Skinner,^{1,2,3,*} C. J. Benmore,² J. K. R. Weber,^{2,3} J. Du,⁴ J. Neuefeind,⁵ S. K. Tumber,³ and J. B. Parise¹

¹*Mineral Physics Institute, Stony Brook University, Stony Brook, New York 11794-2100, USA*

²*X-ray Science Division, Advanced Photon Source, Argonne National Laboratory, Argonne, Illinois 60439, USA*

³*Materials Development Inc., Arlington Heights, Illinois 60004, USA*

⁴*Materials Science & Engineering, University of North Texas, Denton, Texas 76203, USA*

⁵*Spallation Neutron Source, Oak Ridge National Laboratory, Oak Ridge, Tennessee 37831, USA*

(Received 12 September 2013; published 17 April 2014)

The complete set of partial pair distribution functions for a rare earth oxide liquid are measured by combining aerodynamic levitation, neutron and x-ray diffraction on Y_2O_3 , and Ho_2O_3 melts at 2870 K. The average Y-O (or Ho-O) coordination of these isomorphous melts is measured to be 5.5(2), which is significantly less than the octahedral coordination of crystalline Y_2O_3 (or Ho_2O_3). Investigation of La_2O_3 , ZrO_2 , and Al_2O_3 melts by x-ray diffraction and molecular dynamics simulations also show lower-than-crystal cation-oxygen coordination. These measurements suggest a general trend towards lower coordination compared to their crystalline counterparts. It is found that the coordination drop is larger for lower field strength, larger radius cations and is negligible for high field strength (network forming) cations, such as SiO_2 . These findings have broad implications for predicting the local structure and related physical properties of metal-oxide melts and oxide glasses.

DOI: 10.1103/PhysRevLett.112.157801

PACS numbers: 61.20.-p, 61.25.-f, 64.70.dj

Understanding atom-atom interactions in high temperature oxide melts is important to a wide range of fields including nuclear meltdown scenarios [1], the evolution of planetary bodies (particularly Earth's mantle [2]), glass formation [3], and crystal nucleation [4]. Most knowledge of high temperature melt structure has been extrapolated from the study of quenched glasses. Zachariassen's 1932 glass formation rules, for example, classify cations in oxide glasses as network formers, modifiers or intermediates based on their field strength [3,5]. Although modern techniques, such as MAS-NMR have provided detailed oxide glass structure information, far less is known about the structure and properties of high melting point ($T > 2000$ K), non-glass forming oxide liquids such as yttria.

The physical properties of oxide liquids, such as density and viscosity, are largely defined by the local coordination and connectivity between the metal-oxygen (M -O) polyhedra [6]. These polyhedra in oxide liquids and glasses can also take a range of local coordination states, such as AlO_5 units [7,8,11], which are typically not seen in the corresponding crystal structures. However, it does not necessarily follow that the average M -O coordination of these liquids is lower. Although generally lower density than their crystalline counterparts, the packing of the polyhedra, for example, may equally effect the bulk density of oxide liquids. Isolating precise molten M -O coordination information using pair distribution function (PDF) measurements, however, can be challenging due to overlap of the M -O correlations with M - M , and O-O correlations. Despite recent progress [9–11], a full experimental separation of the partial PDFs of a high temperature ($T > 2000$ K) oxide liquid, has not previously been achieved. This is largely due

to the high temperatures required and the limited scattering contrast available from isotope substitution or anomalous scattering methods.

Here, we present a full determination of the M - M , M -O, and O-O partial PDFs for molten Y_2O_3 and its lanthanide isomorphs (Ho_2O_3 , Er_2O_3) with an emphasis on determining the first Y-O peak shape and precise Y-O coordination. Using further x-ray measurements and molecular dynamics (MD) simulations, we also observe a general trend towards lower M -O coordination in a wide range of oxide melts, suggesting that this behavior is a widely occurring phenomenon.

Previous neutron and x-ray diffraction experiments on molten Y_2O_3 reported an average Y-O coordination number, $\bar{n}_{YO} \geq 6.3$ [12–14], whereas MD simulations generally suggest a lower coordination between 4.8 and 5.8 [15–18]. The partial PDF patterns measured in the present work show significant Y-Y and O-O correlations below 3.4 Å (Fig. 2.), which overlap with the first Y-O coordination shell. This overlap explains the higher \bar{n}_{YO} obtained from the previous total scattering measurements, which would count the short O-O and/or Y-Y correlations below 3.4 Å as additional Y-O correlations. This explanation is fully consistent with previous measurements, which used the best available approximations in their Y-O coordination number analysis, but were unable to fully isolate the Y-O partial.

In the present work, high-energy x-ray diffraction measurements were made at 11-ID-C of the Advanced Photon Source, using the aerodynamic levitation sample environment, where the sample is floated on a gas stream and heated with a CO_2 laser described in detail elsewhere [19]. Samples were made from 99.99% (or greater) purity

oxide powders (trace metal basis, Sigma-Aldrich), which were dried at 1000 K for 12 hr immediately prior to weighing. The mixed Y:Ho powders were fused, reground, and fused again twice using a CO₂ laser (Synrad Firestar i401) on a water-cooled Cu plate. Pure O₂ levitation gas was used in the x-ray experiment. The scattered x-ray intensities were measured using a Perkin Elmer XRD1621 area detector and standard correction procedures [20,48].

Neutron diffraction was performed at the NOMAD beam line of the Spallation Neutron Source (SNS) [21], using CO₂ laser heating and aerodynamic levitation as described in Ref. [10]. The sample was levitated using a mixed Ar:O₂ (4% O₂) gas stream, in a chamber which was also filled with the same gas mixture. The measured neutron scattering intensities were normalized to a ~ 3 mm diameter vanadium sphere. To reduce sample attenuation and multiple scattering corrections, the bandwidth choppers were set such that only short incident wavelength neutrons between 0.1–1 Å were used [22]. The final normalization was checked using the expected low- r oscillations and the measured density of 0.058(3) Å⁻³ from [23].

The present measurements utilize the large x-ray scattering contrast (39 vs 67 electrons) and the isomorphic characteristics of molten Y₂O₃ and Ho₂O₃ to extract the partial PDF patterns. For example, their ambient crystal structures are the same, their octahedral ionic radii are 104.0 (Y) and 104.1 pm (Ho) [24], their reported melting temperatures (2712 K, 2688 K) are within 1%, and the volume change on melting is reported to be 11.2% for both Y₂O₃ and Ho₂O₃ [23,25]. Given this isomorphic behavior, diffraction measurements of different mixtures of Y/Ho, give differently weighted x-ray structure factors of essentially the same atomic arrangement. Pure Y₂O₃ and a Y:Ho mixture of 1:2 was used to minimize the multiple scattering and attenuation associated with pure Ho₂O₃. A self-consistency check of the isomorphism was made by confirming the M -O peak (where M represents Y or Ho) canceled out in the x-ray difference pattern [48].

The effect of the mass difference between Ho and Y was also investigated with MD simulations using fixed charge Morse pair potentials. These MD simulations showed no significant difference in the partial PDFs when the mass of the cation was changed from that of Y to Ho. To improve agreement with experiment, initial Y-O and Y-Y potential parameters taken from Refs. [15,16] were refined until maximal agreement between the MD model and the experimental pair distribution function measurements was achieved (see Ref. [48] for final parameters, Fig. 1 for data, and Table I for agreement factors). To maintain consistency across the different M -O melts studied, the OO potential was not refined. The final simulations were run using the DLPOLY classic package [26]. They consisted of 6400 atoms, and were equilibrated at 6000 K for 100 ps, before cooling to 2870 K and running in an NPT ensemble for a further 100 ps, the final system densities were within

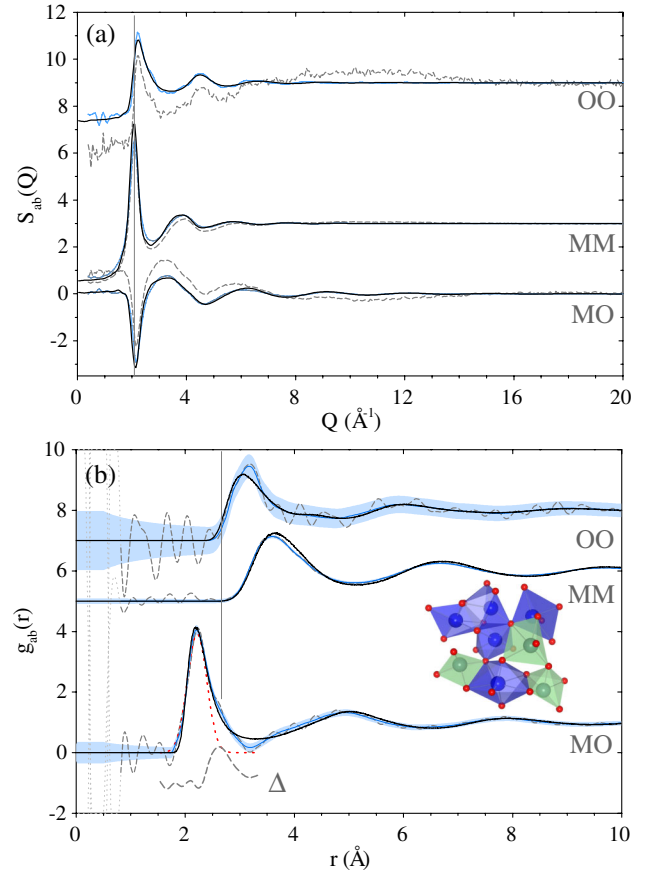


FIG. 1 (color online). (a) Measured partial structure factors of molten M_2O_3 ($M = Y$ or Ho), from raw data (grey dashed line) and back-Fourier transforms (blue lines, correspond to blue lines in b). Black lines are the $S_{ab}(Q)$ patterns for the MD model. (b) Partial pair distribution functions from raw Fourier transform of the measurements (grey dashed line), modified transforms of measurements (blue lines, see Ref. [11] for modification function), error range (light blue shaded area), and the $g_{ab}(r)$'s from the MD model (black lines), all transformed using $Q \leq 18.4$ Å⁻¹. The symmetric red dotted curve represents a Gaussian atom distribution with a $\bar{n}_{MO} = 3.5(5)$, fitted to the low- r side of the M -O peak. This leaves a residual peak centered at 2.56(2) Å, with a $\bar{n}_{MO} = 2.0(5)$ (grey dashed line labeled Δ). Inset is a portion of the MD model, light green polyhedra are YO₄, YO₅, and the dark blue polyhedra are YO₆, YO₇ units. Numerical data provided in Ref. [48].

5% of the measured values [23] (the same MD procedures were repeated for SiO₂, Al₂O₃, ZrO₂, and La₂O₃ melts).

Once corrected, a single diffraction measurement on a one component M -O oxide yields a structure pattern $F(Q)$ which is a linear sum of the three Faber-Ziman partial structure factors, $S_{MM}(Q)$, $S_{MO}(Q)$, $S_{OO}(Q)$, weighted by neutron or x-ray cross-section dependent weightings [29]. To isolate the three partial $S(Q)$ patterns using diffraction, three $F(Q)$ measurements with different weightings were made. The three partial $S(Q)$'s are then related to the three measurements by a matrix $[A]$. For the measurements made in this work, the elements of these matrices are given by

TABLE I. Properties and structure parameters of measured oxides in order of the cation field strength, where field strength is calculated as $Z_M/(r_{MO} - 1.24)^2$, the 1.24 Å represents the O ionic radius [24], and Z is the formal charge of the cation.

	Si-O	Al-O	Zr-O	Y-O	La-O
Field strength ($e/\text{Å}^2$)	26	9.9	5.7	2.9	2.4
r_{MO} (Å) ^a	1.62(1)	1.80(1)	2.08(2)	2.22(2)	2.35(3)
\bar{n}_{MO} (from MD)	4.0(2) ^b	4.5(2)	6.1(4)	5.5(2) ^b	5.9(4)
R_X (%) ^c	3.6	0.8	1.4	0.8	1.3
Temperature (K)	1970	2400	3170	2870	2770
Density (Å ⁻³)	0.066	0.086	0.068	0.058	0.048

^aFrom maximum in $g'(r)$.

^bAgrees with measurements where the first shell was isolated.

^cMD vs diffraction agreement factor in $T_X(r)$ for $1 < r < 8$ Å [27].

$$\begin{bmatrix} F^{X1}(Q) \\ F^{X2}(Q) \\ F^N(Q) \end{bmatrix} = \begin{bmatrix} 0.16f_Y^2 & 0.48f_O f_Y & 0.36f_O^2 \\ 0.16f_x f_x^* & 0.24f_O(f_x + f_x^*) & 0.36f_O^2 \\ 0.16b_Y^2 & 0.48b_O b_Y & 0.36b_O^2 \end{bmatrix} \times \begin{bmatrix} S_{MM}(Q) - 1 \\ S_{MO}(Q) - 1 \\ S_{OO}(Q) - 1 \end{bmatrix}, \quad (1)$$

where f_a is the Q -dependent x-ray form factor of element a (* denotes complex conjugate), the subscript x denotes the Y/Ho 1:2 mixture, and the b 's are the bound coherent neutron scattering lengths (see Refs. [28,29,48] for further detail). Inversion of $[A]$ by singular value decomposition then allows the partial $S(Q)$'s to be obtained. The stability of the solutions to the inverse matrix depends on the contrast between the weightings in each $F(Q)$ measurement. A measure of the stability of inversion is given by normalizing $[A]$ such that each row sums to one, and calculating the determinant of the normalized matrix, $A^n(Q)$ [30]. Low values of $|A^n(Q)|$ indicate uncertain separation of the partial $S(Q)$'s, whereas values approaching ± 1 indicate very well-conditioned separation. The $|A^n(Q)|$ for the liquid M_2O_3 measurements made here is -0.012 (at $Q = 0$). This compares favorably to other recent studies of GeO_2 and SiO_2 glasses [31,32] which had significantly smaller $|A^n(Q)|$ of -0.006 , 0.0021 , respectively (at $Q = 0$).

The measured partial PDFs, $g_{MM}(r)$, $g_{MO}(r)$, $g_{OO}(r)$ obtained from Fourier transform of the partial $S(Q)$ patterns with and without a variable modification are plotted in Fig. 1(b). The variable modification function essentially averages the measurement over an r -dependent width, allowing discrimination against high frequency noise, without significantly broadening the first peaks in the PDF patterns (detailed in Ref. [11]). The first peak in $g_{MO}(r)$ is maximum at $r = 2.22(2)$ Å, and has M -O coordination $\bar{n}_{MO} = 5.5(2)$ measured up to 3.2 Å. This \bar{n}_{MO} , which is significantly less than six, is consistent with previous MD results for molten Y_2O_3 (or Er_2O_3) [15–18].

Figure 1(b) also shows that the O-O and M - M correlations are non-negligible above 2.6 Å, which is well before the end of the first M -O peak [vertical dashed line Fig. 1(b)]. This leads to overlap of M -O, O-O, and M - M correlations between 2.6–3.2 Å in total scattering measurements, and explains the high Y-O coordination numbers ($6.3 < n_{YO} < 7.5$) obtained from previous diffraction measurements on liquid Y_2O_3 .

The first M -O peak is also asymmetric, with additional correlations on the high- r side. Fitting a Gaussian to the low- r side of the M -O peak, gives a $\bar{n}_{MO} = 3.5(5)$ and leaves a residual peak centered at 2.56(2) Å with a $\bar{n}_{YO} = 2.0(5)$ [Fig. 1(b)]. Although other choices of peak fit could be made, this is consistent with the distortion present in the high temperature hexagonal rare earth oxide crystal structures. These hexagonal phases, which precede melting in Y, Ho, and Er oxides, consist of distorted edge shared octahedra and are expected to have a significant fraction of long Y-O bonds in the range 2.4–2.7 Å [25], similar to the hexagonal phases of La_2O_3 and Nd_2O_3 [33,34]. The application of Y/Ho substitution to x-ray pair distribution function measurements applied here, is also valid for studying the detailed local structure of other Y or Ho containing materials.

Beyond Y_2O_3 and its isomorphs, we have measured the x-ray diffraction pattern of several other single-component oxide melts (SiO_2 , Al_2O_3 , ZrO_2 , La_2O_3), and compared these to MD simulations. These other oxide melts represent a range of cation sizes and charges, yet apart from silica, they also have lower \bar{n}_{MO} than their crystalline counterparts (where M represents the metal cations). Figure 2 shows the measured x-ray $T'(r) = 4\pi\rho r g'(r)$ PDF patterns, where ρ is number density, and the ' denotes that the x-ray patterns are reweighted to have equal and r -independent g_{MO} weighting. More specifically, the measured x-ray structure factors, $S_X(Q)$, were scaled such that

$$S'(Q) = [S_X(Q) - 1]w_{MO}(Q)/w_X(Q), \quad (2)$$

where

$$w_{MO}(Q)/w_X(Q) = \frac{c_O c_M f_O (f_M + f_M^*)}{\sum_a c_a f_a \sum_a c_a f_a^*}$$

and where c_a is the concentration of element a , and the sum is over all the chemical species present. The $S'(Q)$ were then transformed to generate the $T'(r)$ patterns plotted in Fig. 2. Note the M - M and O-O contributions are also present, and their weightings vary between each pattern. From Fig. 2 a general trend with increasing cationic field strength can be seen. Where field strength is defined as $Z_M/(r_{MO} - 1.24)^2$, the 1.24 Å represents the O ionic radius [24], and Z_M is the formal charge of the cation (M). The small, high field strength group 3 and 4 elements such as Si, have low \bar{n}_{MO} , and a symmetric first shell. Progressively lower field strength, larger cations, such as Y however,

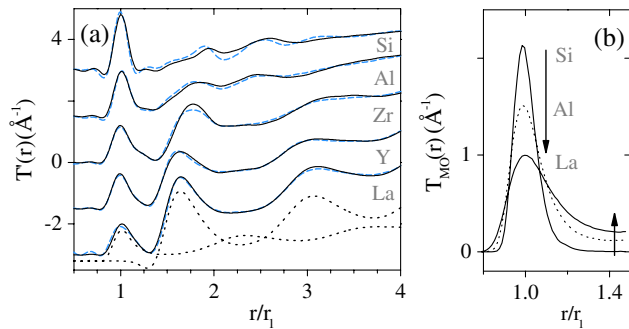


FIG. 2 (color online). (a) Measured x-ray $T'(r) = 4\pi\rho r g'(r)$ pair distribution function patterns (blue dashed lines), where ρ is the number density and the $'$ denotes that the patterns are re-weighted to have equal, r -independent M -O weighting (r_1 is the first M -O peak distance). Black lines are the $T'(r)$ from molecular dynamics (MD) simulations (Q -space patterns and MD potentials given in Ref. [48]). The two dotted curves are the weighted M -O and $MM + OO$ contributions for La_2O_3 . (b) Isolated $T'_{MO}(r)$ from the MD simulations. The arrows indicate decreasing cation field strength.

have higher M -O coordination and more distortion in the first shell. This distortion is observed in the first peak of the liquid PDF patterns as an increasing width and asymmetry with decreasing field strength (Fig. 2). The field strengths, M -O peak positions, and \bar{n}_{MO} are given in Table I.

Figure 3 compares the M -O coordination of these oxide melts to their crystalline counterparts. In addition, the \bar{n}_{MO} is plotted for a wide range of metal cations in oxide glasses [9,16,35–48]. Here, we find that the large radius, low field strength cations have significantly lower \bar{n}_{MO} than their closest corresponding crystals, whereas the low radius, high field strength network formers tend to keep the same coordination.

The coordination of the non- Y_2O_3 melts was obtained from the $g_{MO}(r)$ partial of the MD simulations, which agree with the diffraction $T_X(r)$ measurements to within 4% (see Fig. 2 and Table I). Figure 2(b) also shows that the first peak in $g_{MO}(r)$ only returns to zero on the high- r side for SiO_2 , whereas in all the intermediate and low field strength oxide melts the first coordination shell is less well defined. This result is consistent with the observation that the high field-strength oxides (e.g., SiO_2) maintain the same coordination in the ambient crystal and melt. The majority of oxide melts, however, have lower field strength and less well-defined first coordination shells. These oxides lose a fraction of first shell neighbors in the crystal structures to longer distances outside the first shell in their liquid and glassy states.

The result that M -O coordination in melts and glasses is significantly lower than the corresponding crystalline phase, has several important implications. For example, lower coordination directly affects the expected connectivity between the MO polyhedra: Lower coordinated polyhedra means that on average, the oxygen corners are shared between fewer neighboring polyhedra. Changes in

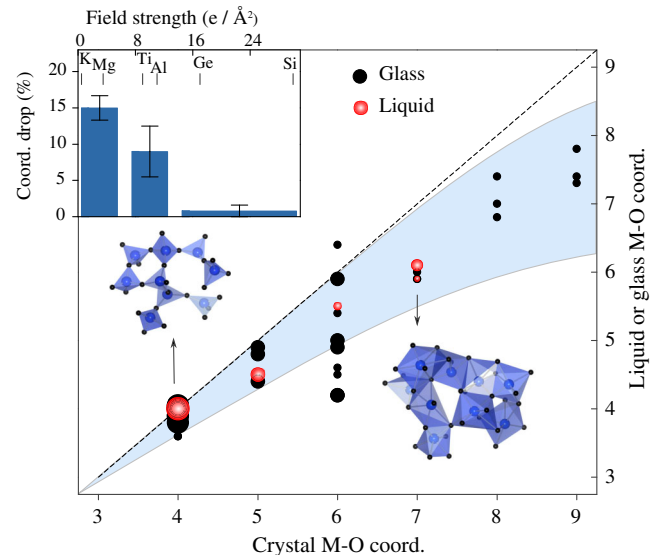


FIG. 3 (color online). The shaded red circles are the \bar{n}_{MO} determinations made from the oxide liquids studied in this work, plotted against \bar{n}_{MO} of their ambient crystal structures. Shaded circle areas are proportional to cation field strength. The solid black circles are literature \bar{n}_{MO} measurements for some representative cations $M = \text{Al, Si, Te, Ge, Ga, Ti, La, Y, Mg, Ca, Sr, Ba, Pb, Na, K}$, in oxide glasses [9,16,35–47] (black circle areas represent large, intermediate or low field strength). The light blue shaded area is a guide to the eye. Inset: Average coordination drop from crystal to the liquid or glass, divided into three groups of, large field strength (network formers), intermediate, and low field strength (modifiers). The atomic configurations correspond to liquid SiO_2 (left) and liquid Y_2O_3 (right) from the MD simulations performed in this work.

this interpolyhedral connectivity and chain length are known to strongly affect properties in the liquid state as well as fragility [6].

The cation-oxygen coordination drop between liquid and crystal phases has previously been noted for several isolated systems [10,11,35]. In this work, however, we find that the trend in M -O coordination number is consistent over a wide range of systems and compositions. Moreover, the M -O coordination number and distortion of the local polyhedra is shown to correlate with field strength for both oxide liquids and glasses.

Our structural findings therefore reinforce the original concepts of ionic field strength on glass formation, which define network modifying and network forming oxides based on their cation field strength [3,5]. As field strength decreases, distortion of local polyhedra increases, and the coordination drops relative to the crystalline phase. It is anticipated that as extreme environment instrumentation and scattering techniques improve, the detailed structure of high temperature melts will be ever more closely linked to their liquid state properties.

Our thanks to R. Spence, J. Carruth, L. Santodonato, C. Fletcher, B. Hill, D. Jin, A. Kadakia and his team for their assistance and expertise. This work was supported by

the U.S. Department of Energy BES DE-FG02-09ER46650 (MD simulations, x-ray experiment, analysis manuscript preparation, L. B. S. and J. B. P.), DOE SBIR DE-SC0004684 (neutron experiment and analysis, L. B. S., C. J. B., J. K. R. W., and S. K. T.) DOE SBIR DE-SC0007564 (partial support of x-ray experiment, J. K. R. W. and S. K. T.). DOE Contracts No. DE-AC02-06CH11357, No. DE-AC05-00OR22725 supported Argonne and Oak Ridge National Laboratories, respectively.

*Corresponding author. lawrie.skinner@gmail.com

- [1] D. R. Olander, *Fundamental Aspects of Nuclear Reactor Fuel Elements: Solutions to Problems* (U.S. Department of Energy, Washington, DC, 1976).
- [2] C. B. Agee, *Phys. Earth Planet. Inter.* **107**, 63 (1998).
- [3] W. H. Zachariasen, *J. Am. Chem. Soc.* **54**, 3841 (1932).
- [4] J. L. Caslavsky and D. J. Viechnicki, *J. Mater. Sci.* **15**, 1709 (1980).
- [5] K.-H. Sun, *J. Am. Ceram. Soc.* **30**, 277 (1947).
- [6] Y. Waseda and J. Toguri, *The Structure and Properties of Oxide Melts* (World Scientific, Singapore, 1998).
- [7] S. K. Lee and J. F. Stebbins, *J. Phys. Chem. B* **104**, 4091 (2000).
- [8] S. Sen and R. E. Youngman, *J. Phys. Chem. B* **108**, 7557 (2004).
- [9] J. W. E. Drewitt, L. Hennem, A. Zeidler, S. Jahn, P. S. Salmon, D. R. Neuville, H. E. Fischer, *Phys. Rev. Lett.* **109**, 235501 (2012).
- [10] L. B. Skinner, C. J. Benmore, J. K. R. Weber, S. Tumber, L. Lazareva, J. Neufeind, L. Santodonato, J. Du, and J. B. Parise, *J. Phys. Chem. B* **116**, 13439 (2012).
- [11] L. B. Skinner *et al.*, *Phys. Rev. B* **87**, 024201 (2013).
- [12] V. Cristiglio, L. Hennem, G. J. Cuello, I. Pozdnyakova, A. Bytchkov, P. Palleau, H. E. Fischer, D. Zanghi, M.-L. Saboungi, and D. L. Price, *J. Non-Cryst. Solids* **353**, 993 (2007).
- [13] L. Hennem, D. Thiaudière, C. Landron, J.-F. Berar, M.-L. Saboungi, G. Matzen, and D. L. Price, *Nucl. Instrum. Methods Phys. Res., Sect. B* **207**, 447 (2003).
- [14] S. Krishnan, S. Ansell, and D. L. Price, *J. Am. Ceram. Soc.* **81**, 1967 (1998).
- [15] A. Pedone, G. Malavasi, M. C. Menziani, A. N. Cormack, and U. Segre, *J. Phys. Chem. B* **110**, 11 780 (2006).
- [16] J. Du, C. J. Benmore, R. Corrales, R. T. Hart, and J. K. R. Weber, *J. Phys. Condens. Matter* **21**, 205102 (2009).
- [17] A. B. Belonoshko, G. Gutierrez, R. Ahuja, and B. Johansson, *Phys. Rev. B* **64**, 184103 (2001).
- [18] L. J. Alvarez, M. A. San Miguel, and J. A. Odriozola, *Phys. Rev. B* **59**, 11303 (1999).
- [19] L. B. Skinner, C. J. Benmore, J. K. R. Weber, M. C. Wilding, S. K. Tumber, and J. B. Parise, *Phys. Chem. Chem. Phys.* **15**, 8566 (2013).
- [20] L. B. Skinner, C. J. Benmore, and J. B. Parise, *Nucl. Instrum. Methods Phys. Res., Sect. A* **662**, 61 (2012).
- [21] J. Neufeind, M. Feyngenson, J. Carruth, R. Hoffmann, and K. K. Chipley, *Nucl. Instrum. Methods Phys. Res., Sect. B* **287**, 68 (2012).
- [22] A. Zeidler, *J. Appl. Crystallogr.* **45**, 122 (2012).
- [23] B. Granier and S. Heurtault, *J. Am. Ceram. Soc.* **71**, C466 (1988).
- [24] R. D. Shannon and C. T. Prewitt, *Acta Crystallogr. Sect. B* **25**, 925 (1969).
- [25] M. Zinkevich, *Prog. Mater. Sci.* **52**, 597 (2007).
- [26] W. Smith and T. R. Forester, *J. Mol. Graphics* **14**, 136 (1996).
- [27] D. I. Grimley, A. C. Wright, and R. N. Sinclair, *J. Non-Cryst. Solids* **119**, 49 (1990).
- [28] H. E. Fischer, A. C. Barnes, and P. S. Salmon, *Rep. Prog. Phys.* **69**, 233 (2006).
- [29] T. E. Faber and J. M. Ziman, *Philos. Mag.* **11**, 153 (1965).
- [30] F. G. Edwards, J. E. Enderby, R. A. Howe, and D. I. Page, *J. Phys. C* **8**, 3483 (1975).
- [31] P. S. Salmon, A. C. Barnes, R. A. Martin, and G. J. Cuello, *J. Phys. Condens. Matter* **19**, 415110 (2007).
- [32] Q. Mei, C. J. Benmore, S. Sen, R. Sharma, and J. L. Yarger, *Phys. Rev. B* **78**, 144204 (2008).
- [33] P. Aldebert and J. P. Traverse, *Mater. Res. Bull.* **14**, 303 (1979).
- [34] J. X. Boucherle and J. Schweizer, *Acta Crystallogr. Sect. B* **31**, 2745 (1975).
- [35] S. Kohara, K. Suzuya, K. Takeuchi, C.-K. Loong, M. Grimsditch, J. K. R. Weber, J. A. Tangeman, and T. S. Key, *Science* **303**, 1649 (2004).
- [36] J. Du and L. René Corrales, *J. Non-Cryst. Solids* **353**, 210 (2007).
- [37] R. L. Mozzi and B. E. Warren, *J. Appl. Crystallogr.* **3**, 251 (1970).
- [38] L. Cormier, G. Calas, S. Creux, P. H. Gaskell, B. Bouchet-Fabre, and A. C. Hannon, *Phys. Rev. B* **59**, 13 517 (1999).
- [39] J. C. McLaughlin, S. L. Tagg, J. W. Zwanziger, D. R. Haefner, and S. D. Shastri, *J. Non-Cryst. Solids* **274**, 1 (2000).
- [40] L. Cormier, P. H. Gaskell, G. Calas, and A. K. Soper, *Phys. Rev. B* **58**, 11 322 (1998).
- [41] A. C. Hannon, J. M. Parker, and B. Vessal, *J. Non-Cryst. Solids* **196**, 187 (1996).
- [42] K. Wezka, A. Zeidler, P. S. Salmon, P. Kidkhunthod, A. C. Barnes, and H. E. Fischer, *J. Non-Cryst. Solids* **357**, 2511 (2011).
- [43] Y. Waseda and J. M. Toguri, *Metall. Mater. Trans. B* **8**, 563 (1977).
- [44] L. Cormier and G. J. Cuello, *Phys. Rev. B* **83**, 224204 (2011).
- [45] L. B. Skinner, A. C. Barnes, P. S. Salmon, H. E. Fischer, J. W. E. Drewitt, and V. Honkimaki, *Phys. Rev. B* **85**, 064201 (2012).
- [46] M. C. Eckersley, P. H. Gaskell, A. C. Barnes, and P. Chieux, *Nature (London)* **335**, 525 (1988).
- [47] M. C. Wilding, C. J. Benmore, J. A. Tangeman, and S. Sampath, *Europhys. Lett.* **67**, 212 (2004).
- [48] See Supplemental Material at <http://link.aps.org/supplemental/10.1103/PhysRevLett.112.157801> for further diffraction details, measured data, literature coordination number data, MD potential parameters.